Real time equilibrium reconstruction for tokamak discharge control

1998 Nucl. Fusion 38 1055

(http://iopscience.iop.org/0029-5515/38/7/308)

REAL TIME EQUILIBRIUM RECONSTRUCTION FOR TOKAMAK DISCHARGE CONTROL

J.R. FERRON, M.L. WALKER, L.L. LAO,
H.E. ST. JOHN, D.A. HUMPHREYS, J.A. LEUER
General Atomics,
San Diego,
California,
United States of America

ABSTRACT. A practical method for performing a tokamak equilibrium reconstruction in real time for arbitrary time varying discharge shapes and current profiles is described. An approximate solution to the Grad–Shafranov equilibrium relation is found which best fits the diagnostic measurements. Thus, a solution for the spatial distribution of poloidal flux and toroidal current density is available in real time that is consistent with plasma force balance, allowing accurate evaluation of parameters such as discharge shape and safety factor profile. The equilibrium solutions are produced at a rate sufficient for discharge control. This equilibrium reconstruction algorithm has been implemented on the digital plasma control system for the DIII-D tokamak. The first application of real time equilibrium reconstruction to discharge shape control is described.

1. INTRODUCTION

Optimum performance of a tokamak discharge requires accurate feedback control of many of the discharge parameters. For this to be possible, the values of these parameters must be accurately measured. The values of many discharge parameters, such as shape and safety factor profile, are not directly measured but can be evaluated from the available diagnostic data: magnetic field and flux measurements, for example. The most complete evaluation comes from fitting the diagnostic data to the Grad–Shafranov model, which describes the force balance of the tokamak equilibrium, while allowing for a distributed current source. This full reconstruction of the equilibrium has normally been performed off-line using a computation intensive fitting algorithm [1]. To compute discharge parameters in real time rapidly enough for use in tokamak feedback control, simpler algorithms implemented at most tokamak facilities [2–9] approximate the results of the full equilibrium reconstruction. The accuracy of the approximations is limited, though, because the models do not include the force balance of the plasma and do not allow a solution with current distributed throughout the plasma volume, so that the plasma current distribution cannot be correctly calculated.

This article describes a practical method for performing an equilibrium reconstruction in real time for arbitrary time varying discharge shapes and current profiles. An approximate solution to the Grad–Shafranov equilibrium relation is found that best fits the diagnostic measurements so that an equilibrium solution consistent with force balance, expressed in terms of the spatial distributions of the toroidal current density and poloidal flux, is available in real time for accurate evaluation of the discharge parameters. The solutions are produced at a rate sufficient for discharge control. The computed values of the discharge parameters agree well with the results from the best off-line calculations because a similar algorithm is used. This equilibrium reconstruction algorithm has been implemented on the digital plasma control system [10, 11] for the DIII-D tokamak [12], and we describe here its first application for tokamak discharge control.

Discharge parameters that can be important for tokamak performance optimization include the shape, electron density, total plasma current and stored energy. In advanced tokamak scenarios, control of more detailed parameters such as safety factor profile, pressure profile, internal inductance and beta may be required. The equilibrium reconstruction algorithm described here will provide accurate results for the evaluation of all of these parameters. Shape identification with this reconstruction technique is robust to changes in the shape, β_p, ℓ_i and edge current density. Motional Stark effect (MSE) diagnostic data can be included in the equilibrium reconstruction [13] to provide the measurements internal to the plasma that allow additional details of the toroidal current density profile to be determined. So, for instance, the strong effect of the solution for the current density near the discharge edge on the calculated X point location

[11] can be properly handled. In addition, the safety factor profile can be calculated in real time.

In this article, we describe the use of the equilibrium reconstruction algorithm for identification of the discharge shape and the concept for the way in which the results of the shape identification are used for discharge shape control. The important characteristics of the discharge shape include whether or not there is a poloidal divertor, the number and location of X points, the distance between the last closed flux surface and the vacuum vessel walls, the elongation, triangularity, major and minor radii, and the location where the divertor separatrix flux surface strikes the vessel wall. These characteristics influence tokamak performance in areas such as the magnetohydrodynamic (MHD) stability properties, the location where the heat lost from the discharge is deposited on the vessel wall, whether the vertical position can be controlled and the loading resistance for radiofrequency heating antennas. Precise control of the X point and strike point positions is particularly important in closed divertor configurations where field lines must pass through relatively small gaps in divertor structures.

The algorithms described previously that are intended to provide shape identification rapidly enough for real time control take approaches that differ significantly from a full equilibrium reconstruction. Some of these algorithms use regression analysis to fit some function of the diagnostic measurements to one or more of the discharge shape parameters (e.g., major radius or elongation) [3–5]. The function is chosen for ease of evaluation in real time. Examples of this method are neural networks [6] and function parametrization [8]. These methods use as input to the regression analysis a database of equilibria that defines the range of equilibria that the function can represent. A second class of algorithms uses a small set of filaments or finite elements to represent the plasma current, allowing the poloidal flux at any location to be calculated [2, 7]. These currents are derived in real time from the product of the diagnostic values and the inverse of the matrix giving the response of the diagnostic measurements to currents in the filament set. The number of elements in the set is limited by the conditioning of the matrix inversion. The third class of shape approximation algorithms uses a local expansion of the field to extrapolate from diagnostic locations to the discharge boundary [9].

It is still not possible to execute in real time the exact algorithm used for the best off-line equilibrium reconstructions. However, the speeds of present day digital processors allow an algorithm very close to that described in Ref. [1] to be executed on a timescale fast enough for shape control in the DIII-D tokamak. Relative to the shape control accuracy that can be achieved and the uncertainties introduced by diagnostic accuracy, the results from the real time algorithm do not differ significantly from those of the full off-line analysis. For instance, in the examples shown in this article, the differences in the computed boundary location are less than a few millimetres.

We describe here the features of the algorithm that make real time execution possible, the accuracy of the real time algorithm and the way this algorithm has been used for discharge shape control in the DIII-D tokamak. In Section 2, the concept for use of the shape identification results in control is described in order to establish the requirements for the equilibrium reconstruction algorithm. An outline of the reconstruction algorithm is given in Section 3, and in Section 4 the modifications necessary for real time execution are described. An analysis of the consequences of these modifications is presented. In Section 5 examples of the performance of the real time reconstruction algorithm during discharge control are given. In the concluding section (Section 6) is a discussion of improvements that could be made in the algorithm and the corresponding requirements on computation speed. The Appendix provides a brief description of the implementation of the algorithm for the DIII-D tokamak.

2. SHAPE CONTROL METHOD

The shape control method used with the equilibrium reconstruction algorithm is the 'isoflux' technique [14], in which a set of locations is specified that define the desired plasma boundary and the poloidal field coil currents are adjusted to keep the poloidal flux equal at all of these locations. This is illustrated in Fig. 1 where, for the case of a single null divertor discharge shape, the diamonds indicate the 'control points', locations at which the value of the flux is controlled. The equilibrium reconstruction algorithm is used to calculate the values of the flux at the control points.

The set of control points is chosen to constrain the characteristic shape parameters. In this single null divertor case these are the major radius, the gaps between the inside and top surfaces of the vessel and the separatrix flux surface, the X point radial and vertical positions, and the triangularity of the top half of the discharge. Because the control is not based on

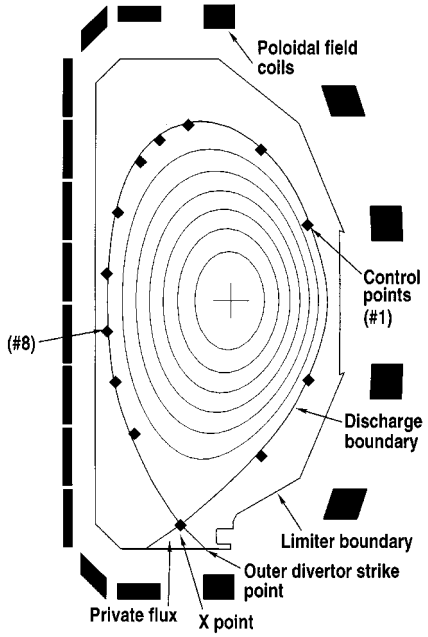

FIG. 1. Example of a single null divertor discharge (No. 90291 at 2.5 s) produced using the isoflux control method in combination with real time equilibrium reconstruction. The diamonds show the locations of the control points.

errors in these shape parameters, but rather on errors in a local poloidal flux value, it is not necessary to compute the location of the plasma boundary during the equilibrium reconstruction.

One of the control points is chosen as the reference, and the flux at the other points is controlled to be equal to the value at the reference point. To ensure that the flux surface on which the control points lie is actually the discharge boundary, the reference point is chosen to be one that, for the particular type of discharge to be produced, must by definition lie on the boundary. For instance, for a discharge that is intended to have the boundary limited by the vessel wall, the intended point of intersection with the vessel wall is used as the reference point. In a divertor discharge the X point locations are controlled directly. The actual X point locations are determined by finding the locations where $|\boldsymbol{B}_\mathrm{p}| = 0$, and the coil currents are adjusted to move the X point to the intended location. For single null divertor discharges, the actual X point location is then used as the reference point. In a double null divertor case, the flux at one of the X point locations is used as the reference and the flux at the other X point location is adjusted to be equal to the reference flux.

To facilitate calculation of the flux at the control points, the equilibrium reconstruction algorithm models the plasma current as being distributed on a large set of rectangular current elements arranged on a rectangular grid and solves for the current in each element (Section 3). The total poloidal flux at a control point or the poloidal field near an X point can be found from the sum of the individual contributions from the current in each of these rectangular regions, the currents in the external field coils and the induced currents in the vessel and support structures. The proportionality coefficients can be precalculated to form a 'response vector'. The real time calculations of flux or field then require only dot products of the response vectors with the vector of the toroidal currents.

3. OUTLINE OF THE EQUILIBRIUM RECONSTRUCTION METHOD

The task of the equilibrium reconstruction algorithm [1] is to compute the distributions in the R, Z plane of the poloidal flux, ψ, and the toroidal current density, J_t, that provide a least squares best fit to the diagnostic data and that simultaneously satisfy the model given by the Grad–Shafranov equation

$$\Delta^* \psi_\mathrm{p} = -\mu_0 R J_\mathrm{t}(R, \psi). \tag{1}$$

Here the total poloidal flux is $\psi = \psi_\mathrm{p} + \psi_\mathrm{coil}$, where ψ_p is the poloidal flux resulting from the plasma current and ψ_coil is the poloidal flux generated by current in the sources external to the plasma. For the DIII-D tokamak, the diagnostic data consist of measurements of flux and field outside the plasma, plasma current from a Rogowski loop, internal field line pitch angle measurements made with the MSE diagnostic and current in the poloidal field and ohmic heating coils.

The equilibrium solution consists of values of ψ and J_t on a rectangular grid that covers the entire area of the vacuum vessel. The current is modelled as being distributed among a set of rectangular elements, one centred at each grid point, with the total number of grid points being typically 1000 or more. The large number of grid points allows the solution to provide a realistic distribution of the current density, including provision for finite current density at the discharge edge. The current density is modelled, however, by only a small number of free parameters,

$$J_\mathrm{t}(R, \psi; \boldsymbol{\alpha}_J, \boldsymbol{\gamma}_J, \delta_Z) = R\left(P'(\psi; \boldsymbol{\alpha}_J, \delta_Z) + \frac{\mu_0 F F'(\psi; \boldsymbol{\gamma}_J, \delta_Z)}{4\pi^2 R^2}\right) \tag{2}$$

where P is the plasma pressure, F is related to the poloidal current, primes indicate total derivatives with respect to poloidal flux and $\boldsymbol{\alpha} = (\boldsymbol{\alpha}_J, \boldsymbol{\gamma}_J, \delta_Z)$ is the set of free parameters in the plasma current model. Polynomials are often used to provide basis functions for P' and FF',

$$P'(\psi, R, Z) = \sum_{n=0}^{n_P} \alpha_n \left(\psi_\mathrm{N} + \frac{\partial \psi_\mathrm{N}}{\partial Z} \delta_Z \right)^n \tag{3}$$

$$FF'(\psi, R, Z) = \sum_{n=0}^{n_F} \gamma_n \left(\psi_\mathrm{N} + \frac{\partial \psi_\mathrm{N}}{\partial Z} \delta_Z \right)^n \tag{4}$$

where $\boldsymbol{\alpha}_J = (\alpha_0, \alpha_1, \ldots, \alpha_{n_P})$ and $\boldsymbol{\gamma}_J = (\gamma_0, \gamma_1, \ldots, \gamma_{n_F})$. Here $\psi_\mathrm{N} = (\psi - \psi_\mathrm{axis})/(\psi_\mathrm{bdy} - \psi_\mathrm{axis})$ is the flux normalized to the flux difference from the centre to the edge of the discharge, ψ_axis is the flux at the magnetic axis and ψ_bdy is the flux at the last closed flux surface. The normalized flux, ψ_N, provides an adjustable mapping from the small number of fitting parameters to the large number of grid points on the R, Z plane.

The free parameter δ_Z in the current profile model provides the freedom to adjust the vertical position of the equilibrium during the calculation of the least squares solution by allowing an approximately rigid vertical shift of the ψ_N distribution. In the real time algorithm (Section 4), this allows the equilibrium reconstruction to follow the vertical movement of the discharge. Because of the δ_Z term, however, the basis functions in Eqs (3) and (4) have R and Z dependences that do not conform to the Grad–Shafranov model. In a good equilibrium solution, ψ_N used in the basis functions differs little from ψ_N in the solution, so that the fitted value of δ_Z is close to zero. In this case, the R and Z dependences in Eqs (3) and (4) are small and the difference between the right and left hand sides of Eq. (1) is of the order of the numerical accuracy of the calculation.

The currents in the external poloidal field coils are also free parameters in the fitting problem and, potentially, the induced currents in the vacuum vessel and support structures can be treated in this way as well. Direct measurements of the external coil currents are used as constraints on the solution. Thus, the total vector of unknowns for the fitting problem is

$$\boldsymbol{U} = (\boldsymbol{I}_\mathrm{c}, \boldsymbol{\alpha}) \tag{5}$$

where $\boldsymbol{I}_\mathrm{c}$ is the vector of external current sources.

For a fixed value of $\boldsymbol{\psi}_\mathrm{N}$, the vector of values of the normalized flux at each of the grid points, the least squares best fit result for $\boldsymbol{U}$ is found by inverting the weighted response matrix,

$$\boldsymbol{U} = (\boldsymbol{F} \cdot \mathbf{R})^{-1} \times (\boldsymbol{F} \cdot \boldsymbol{D}) \tag{6}$$

where the operator '$\cdot$' indicates multiplication of each column of the matrix by the vector. The response matrix, $\mathbf{R}$, relates the fitting parameter vector to the vector of diagnostic measurements, $\boldsymbol{D}$,

$$\boldsymbol{D} = \mathbf{R} \times \boldsymbol{U} \tag{7}$$

and the fitting weight vector, $\boldsymbol{F}$, has one element for each diagnostic signal equal to the inverse of the measurement uncertainty.

The basis functions for the plasma current model are collected into the response matrix. The component of the right hand side of Eq. (7) resulting from the plasma current is $\mathbf{G}_\mathrm{p} \times \boldsymbol{I}_\mathrm{p}$, where $\mathbf{G}_\mathrm{p}$ contains the Green's function coefficients relating current at the grid elements to signal at the diagnostics. The plasma current at the grid elements is

$$\boldsymbol{I}_\mathrm{p} = \boldsymbol{\Psi} \times \boldsymbol{\alpha}. \tag{8}$$

The matrix $\boldsymbol{\Psi}$ contains the basis functions, the coefficients of the elements of $\boldsymbol{\alpha}_J$ and $\boldsymbol{\gamma}_J$ from Eqs (3) and (4),

$$\boldsymbol{\Psi} = \left(\boldsymbol{R}, \boldsymbol{R}\psi_\mathrm{N}, \ldots, \boldsymbol{R}\psi_\mathrm{N}^{n_P}, \frac{1}{\boldsymbol{R}}, \frac{\boldsymbol{\psi}_\mathrm{N}}{\boldsymbol{R}}, \ldots, \frac{\psi_\mathrm{N}^{n_F}}{\boldsymbol{R}}, \boldsymbol{C}_{\delta_Z} \right) \tag{9}$$

where $\boldsymbol{R}$ is the vector of values of the major radius at the grid points and the terms linear in δ_Z are collected into $\boldsymbol{C}_{\delta_Z}$. Thus, the largest component of the response matrix, $\mathbf{G}_\mathrm{p} \times \boldsymbol{\Psi}$, represents the contribution of the plasma current.

The vector of all axisymmetric current sources, $\boldsymbol{I}_\mathrm{axi} = [\boldsymbol{I}_\mathrm{c}, \boldsymbol{I}_\mathrm{p}]$, is assembled from the solution for $\boldsymbol{U}$ and Eq. (8). From $\boldsymbol{I}_\mathrm{axi}$ the vector of values of total flux at the grid points, $\boldsymbol{\psi}$, is calculated. Using $\boldsymbol{\psi}$, the plasma boundary and magnetic axis can be located to obtain values for ψ_bdy and ψ_axis and to calculate a new value for $\boldsymbol{\psi}_\mathrm{N}$ corresponding to the new value of $\boldsymbol{I}_\mathrm{axi}$.

In the off-line equilibrium reconstruction algorithm [1], the solution is iterated by using the new value of $\boldsymbol{\psi}_\mathrm{N}$ to compute new values for $\mathbf{R}$, $\boldsymbol{U}$, $\boldsymbol{I}_\mathrm{axi}$ and $\boldsymbol{\psi}$. This iteration process continues until the solution has converged, as indicated by the largest change in an iteration of the value of ψ at any grid point being less than a threshold value.

With present day computing hardware it is not possible to obtain the well-converged solution on the

millisecond time-scale required for discharge shape control. The processes of computing $\mathbf{G}_p \times \boldsymbol{\Psi}$, $\boldsymbol{\psi}$ and inverting $\boldsymbol{F}\cdot\mathbf{R}$ are particularly computationally intensive. The next section describes the real time version of the algorithm that obtains solutions at the necessary rate.

4. THE REAL TIME ALGORITHM

In the real time version of the equilibrium reconstruction algorithm, the time consuming process of iterating to a well-converged solution for a fixed set of diagnostic data is eliminated. Instead, for each new reconstruction a new set of diagnostic data is acquired, the most recent equilibrium solution is used as the starting point and one iteration is performed. If the equilibrium is not evolving too quickly, the changes since the previous solution can be accounted for in one iteration so that the result has an accuracy sufficient for discharge control. The adequacy of a one iteration solution is demonstrated in this section, and other time saving changes to the algorithm are described.

The real time reconstruction algorithm is divided into two portions. The first is the relatively fast shape control computation loop in which the first portion of an equilibrium reconstruction iteration, resulting in $\boldsymbol{I}_{axi}$, is executed and the shape control power supply commands are generated. Each solution for $\boldsymbol{I}_{axi}$ represents a one iteration equilibrium reconstruction. The input to the shape control loop is the $\mathcal{S}$ data set, $\mathcal{S} = \{(\boldsymbol{F}\cdot\mathbf{R})^{-1},\ \boldsymbol{\Psi},\ \boldsymbol{F}\}$. Given $\mathcal{S}$, only two relatively small matrix multiplications (Eqs (6) and (8)) are required to obtain $\boldsymbol{I}_{axi}$. The calculations of the flux values at control points, the field values near the X points and the X point locations are rapid, involving primarily a small number (about 20 for DIII-D) of dot products between the response vectors for flux or field at control points and $\boldsymbol{I}_{axi}$. Each time this shape control loop is executed a new set of diagnostic data is obtained, but the same value of the $\mathcal{S}$ data set will be reused until a new data set is prepared.

The second portion of the algorithm (the 'slow' loop) completes the steps required in a reconstruction iteration by preparing a new $\mathcal{S}$ data set. This involves significant computation, requiring approximately 25 times longer than the shape control loop, which is why the shape control loop must reuse $\mathcal{S}$ many times. As part of this process, the flux vector $\boldsymbol{\psi}$ is obtained, defining along with $\boldsymbol{I}_{axi}$ the complete equilibrium solution. Quantities such as the safety factor profile, poloidal beta, internal inductance, etc., which are obtained using $\boldsymbol{\psi}$, can be computed at this point. Immediately after $\mathcal{S}$ is computed it is provided to the shape control loop. The first result for $\boldsymbol{I}_{axi}$ obtained using the new $\mathcal{S}$ is used as input to the next computation of an updated $\mathcal{S}$ data set. Thus, the shape control loop uses a starting point data set based on diagnostic data sampled $\tau_{\mathcal{S}}$ to $2\,\tau_{\mathcal{S}}$ earlier, where $\tau_{\mathcal{S}}$ is the time required for the calculation of $\mathcal{S}$.

In addition to performing only one iteration, there are other modifications made to the reconstruction algorithm in order to increase the calculation speed. First, if the discharge shape is well controlled, the boundary should be located very near the reference control point, so to determine the flux at the discharge boundary the flux at the reference control point is used. This avoids the complex boundary tracing routine used by the off-line reconstruction algorithm. To determine ψ_{axis} the peak value of the flux at a grid point is used. Because $\nabla\psi$ in the region near the magnetic axis is small, this method yields a value with a very small difference from the value obtained from the more complex algorithm that searches for the peak in poloidal flux. The time to calculate $\mathcal{S}$ is strongly influenced by the number of elements in the vector of fitting parameters $\boldsymbol{U}$. A direct measurement of the currents in each of the poloidal field coils is available, allowing these values to be treated as known rather than treating them as fitting parameters. This is implemented by subtracting the contributions of the coil currents to the diagnostic measurements from $\boldsymbol{D}$ before the fitting is performed. In this case, then, $\boldsymbol{I}_c$ is not a component of $\boldsymbol{U}$. For DIII-D, the number of elements in $\boldsymbol{I}_c$ is up to 24 while the typical number of elements in $\boldsymbol{\alpha}$ is 4 to 8, so treating the coil currents as known values causes a large change in the number of free parameters. Finally, if necessary, both the number of points on the calculation grid and the number of diagnostics used in the fit can be reduced to decrease the calculation time.

A premise of the real time algorithm is that if the differences between the starting point equilibrium (represented by $\mathcal{S}$) and a well-converged reconstruction are small enough then after only one iteration the solution will be close enough to the well-converged reconstruction to be adequate for discharge control. An additional premise is that one iteration will be sufficient to allow the real time algorithm to follow changes in the equilibrium as the discharge evolves. To test these premises, two off-line calculations were performed to evaluate, for DIII-D conditions, the

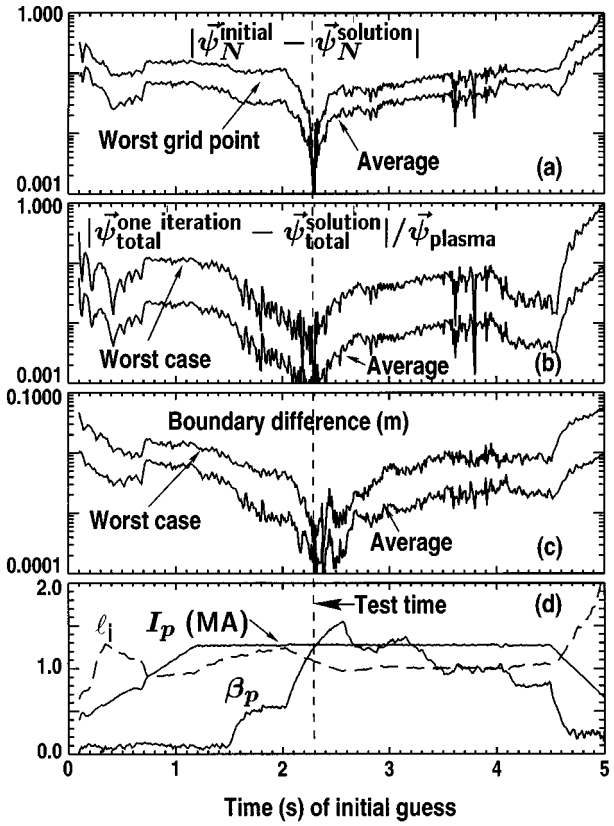

FIG. 2. Test of the effect of variation of the starting point equilibrium on the one iteration reconstruction solution. Results are plotted versus the time from which an equilibrium was obtained to use as an initial guess for the one iteration solution. (a) Difference between the normalized flux at the grid points for the initial guess and a well-converged result at the reference time. Both the largest value at an individual grid point and the average of all grid points are shown. (b) Difference between the total flux on the grid for the one iteration solution and the well-converged solution at the reference time normalized to the difference between the flux on the axis and the flux at the discharge boundary. (c) The gap between the discharge boundaries as determined by the one iteration solution and the well-converged solution at the reference time. (d) Total plasma current, I_p, poloidal beta, β_p, and internal inductance, ℓ_i (dashed curve), for the test discharge shown to illustrate the periods of the discharge when the equilibrium is evolving relatively quickly.

effect of varying the starting point equilibrium on the accuracy of a one iteration solution and to test how well the real time algorithm follows the time evolution of a discharge.

The results of a test of the accuracy of a one iteration solution as a function of the starting point equilibrium are shown in Fig. 2. The test was performed by choosing a single time slice in a discharge (here at 2.3 s) as the reference time and comparing a well-converged solution obtained using data from that time slice with a variety of one iteration solutions for that time slice. Each one iteration solution was produced by using ψ_N from the reconstructed equilibrium for a different time slice in the same discharge to compute the $\mathcal{S}$ data set. Recall that the $\mathcal{S}$ data set is used as the starting point for a one iteration solution. The solution starting point in this test always has, then, parameters somewhat similar to the parameters at the reference time slice, as would be the case in the real time algorithm, but there is a variation in the starting point that results from variations in the plasma current, poloidal beta and internal inductance throughout the discharge (Fig. 2(d)). The data shown in Figs 2(a) to (c) are the results of one iteration solutions of the equilibrium at the time slice 2.3 s plotted versus the time from which the data to produce the starting point equilibrium were obtained.

The results of this test show that it is reasonable to expect that a single iteration solution can be sufficiently close to the well-converged result. First, Fig. 2(a) compares the starting point equilibrium used to obtain the one iteration solution to the well-converged solution. The compared quantity is the normalized flux on the grid, since that is the fundamental quantity defining the initial guess for the reconstruction problem. Because the poloidal beta, and thus the equilibrium, is evolving rapidly at the reference time, the difference in normalized flux increases rapidly as the difference between the time from which the starting point equilibrium was taken and the reference time increases. The largest difference in flux is with equilibria from periods when the plasma current is changing rapidly. However, as long as a starting point equilibrium is obtained from a time slice within a few hundred milliseconds of the reference time, the initially guessed flux values differ from those of the reference time by only a few per cent on average. Figure 2(b) shows the normalized difference in total flux between the one iteration and the well-converged solutions. This is the quantity used in the full equilibrium reconstruction to test for convergence of the solution. For starting point equilibria originating within 100 to 200 ms of the reference time, the average of this value is near 1×10^{-3}. This is comparable to the maximum acceptable value for the convergence test, indicating that the one iteration solution is reasonably accurate. The 'worst case' curve in Fig. 2(b) comes from grid points near the magnetic axis, so that the flux near the boundary would be expected to be characterized by the average

differences. For the period when the plasma current is constant, the quantities in Figs 2(a) and (b) can be compared quantitatively, showing that the single iteration improves the flux distribution accuracy by a factor of 2 to 8, depending on the starting point equilibrium.

For shape control, the most relevant issue is how accurately the discharge boundary is determined. Figure 2(c) compares the distance between the discharge boundary determined from the one iteration solution and the boundary from the well-converged solution. For starting point equilibria taken from a time within 100 to 400 ms of the reference time, the difference is less than one millimetre, adequate for shape control and less than the boundary location uncertainty resulting from uncertainties in the diagnostic measurement values [1]. Overall, in this test case a one iteration solution is sufficiently accurate as long as the real time algorithm can use an equilibrium as the reconstruction starting point that results from data acquired within a few hundred milliseconds of the current time.

In order to assess the impact of the finite time required to calculate the $\mathcal{S}$ data set, $\tau_{\mathcal{S}}$, off-line simulations of the real time algorithm were performed with different values of $\tau_{\mathcal{S}}$. The simulation also produced predictions for the reconstruction accuracy that could be expected from the real time algorithm. Data from a previously produced DIII-D discharge were used to simulate the data that would be acquired in real time. In the shape control loop portion of the simulation the result for $\boldsymbol{I}_{\mathrm{p}}$ was saved for further analysis; ψ was calculated from $\boldsymbol{I}_{\mathrm{p}}$ and the discharge boundary location was traced to provide a record of the prediction of the discharge boundary by the real time algorithm. In addition, a well-converged equilibrium reconstruction was calculated for comparison with the results of the real time algorithm.

As $\tau_{\mathcal{S}}$ is increased in the simulation, the difference in the computed boundary location between the real time algorithm and the well-converged reconstruction increases first during periods of the discharge when the equilibrium is changing rapidly. This is illustrated in Fig. 3, which shows results for $\tau_{\mathcal{S}} = 10$ ms and $\tau_{\mathcal{S}} = 50$ ms for the sample DIII-D discharge. During the period of constant plasma current the average difference in the boundary location is typically less than 1 mm (Fig. 3(c)). There is no significant effect of changing $\tau_{\mathcal{S}}$ on the difference during the period of the rapid rise in poloidal beta that begins at 2 s nor during the rapid 10 to 20% drop in poloidal beta at 2.55 s. However, during the rampup and rampdown of

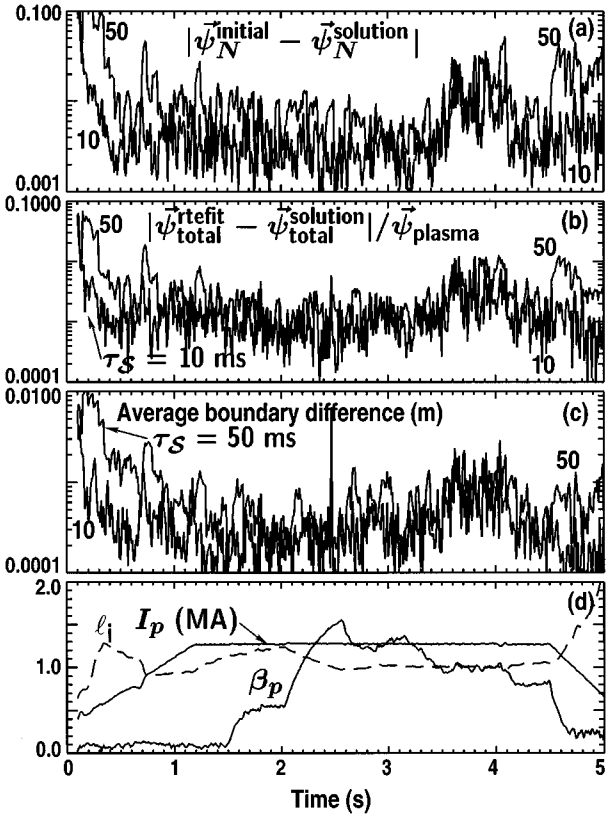

FIG. 3. Simulation of the real time algorithm made using data from the same discharge used for Fig. 2. The same quantities shown in Fig. 2 are shown here. In this example, the results compared at each time slice are those from the real time algorithm simulation and those from a well-converged reconstruction. Only the average values are shown. The real time algorithm was simulated with two values of $\tau_{\mathcal{S}}$: 10 and 50 ms. At the beginning and end of the discharge the two curves are labelled; these are the only periods when there is an easily discernible difference.

the plasma current, when the current profile is changing rapidly, the boundary position error is increased by a factor of between 5 and 10 to values as high as 1 cm by increasing $\tau_{\mathcal{S}}$ from 10 to 50 ms.

The simulated results for the flux distribution are generally in agreement within a few tenths of a per cent with the solution found by the well-converged reconstruction (Fig. 3(b)). This should allow for good accuracy in real time computation of quantities such as safety factor profile, poloidal beta and internal inductance. The normalized flux values in the starting point equilibrium at each time slice are already in agreement with the well-converged result within approximately 0.01 (where the maximum difference is 1.0) (Fig. 3(a)), which is why a

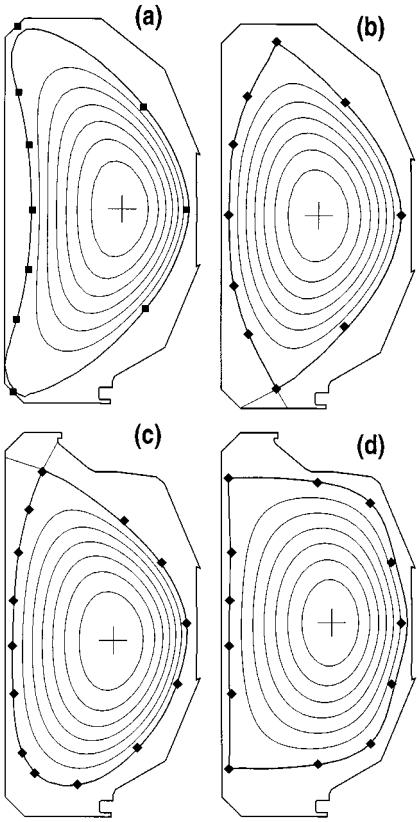

FIG. 4. Examples of the variety of discharge shapes produced in the DIII-D tokamak using the isoflux control algorithm combined with the real time equilibrium reconstruction: (a) crescent/bean shaped, (b) low triangularity double null divertor, (c) upper single null divertor, (d) square shaped double null divertor. The diamonds show the locations of the control points.

reconstruction obtained after only one iteration is still quite accurate.

5. APPLICATION TO SHAPE CONTROL IN THE DIII-D TOKAMAK

The real time equilibrium reconstruction algorithm combined with the isoflux technique has been used to control a variety of discharge shapes in the DIII-D tokamak. Some examples are shown in Figs 1 and 4. The differences in control of these shapes are the power supply configuration for the poloidal field coils, the choice of the set of control points and the choice of control gains for the commands to the coil power supplies. Otherwise the isoflux control algorithm is similar for all cases, following the scheme described in Section 2, and the same equilibrium reconstruction algorithm is used. Thus, it is relatively easy to create, using this control scheme, the variety of discharge shapes required by the research programme. In this section, we use the single null divertor discharge shown in Fig. 1 as an example, focusing on results from the real time equilibrium reconstruction. Work to improve the controller design, which affects the ability to control the coil currents in an optimum manner in order to place the boundary at the control points, will be reported in the future.

Experience with DIII-D discharges controlled with the isoflux algorithm shows that the real time equilibrium reconstruction yields results with the good accuracy predicted by the simulations discussed in Section 4. This is illustrated by the comparisons shown in Fig. 5 between the real time result and the result from the full equilibrium reconstruction calculated off-line. Comparisons are made of the X point position and values of the flux at the control points. The sample discharge has a preprogrammed sweep of the X point position (Figs 5(a) and (b)) during which the two equilibrium reconstructions agree on the X point location within a few millimetres (Fig. 5(c)). The two computations of the flux at the control points agree to within less than 1×10^{-3} V · s/rad. To put this value in perspective, it is displayed in Figs 5(d) and (e) for two of the control points as a distance computed from $(\psi_{\text{real time}} - \psi_{\text{off-line}})/(\partial\psi/\partial\ell)$, where $\psi_{\text{real time}}$ and $\psi_{\text{off-line}}$ are the flux values computed in real time and off-line, respectively, and the flux derivative is taken along a line between the control point and the magnetic axis. This quantity is approximately the difference in the predictions by the two calculations of the boundary location in the region of the control point. Throughout the discharge, this difference is of the order of a few millimetres, about 0.5% of the 0.62 m typical plasma minor radius.

Differences between the real time and off-line results are primarily a result of differences in how well the calculation is converged and differences in how the currents in the poloidal field coils are treated. The comparisons shown in Fig. 5 were obtained using exactly the same diagnostics and current profile model for both the real time and the off-line cases. In Figs 5(d) and (e) the dashed curves show the results obtained from treating, in both calculations, the currents in the poloidal field coils as known values, as is normally the case for the real time algorithm. Thus, differences in the results reflect primarily the effect of performing only one iteration for each reconstruction. The best off-line calculation includes the poloidal field coil currents as free fitting

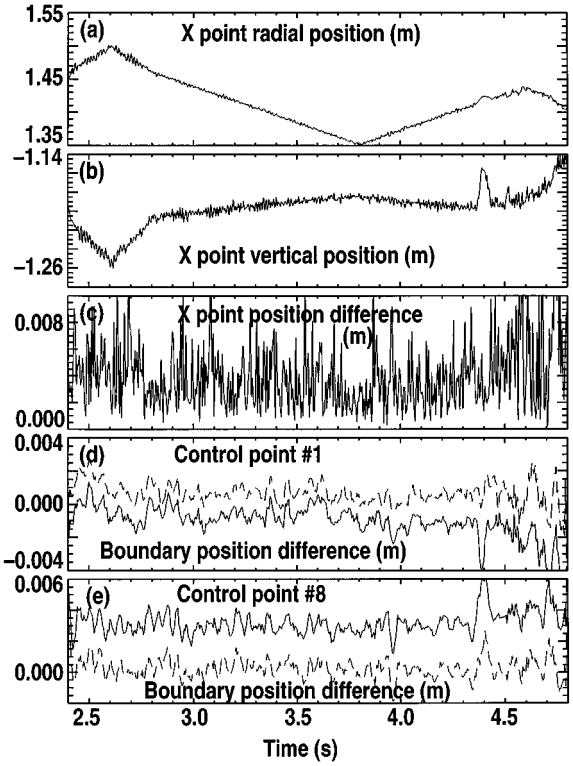

FIG. 5. Comparison of the results from the real time equilibrium reconstruction for the discharge shown in Fig. 1 with the results from well-converged solutions from off-line calculations. (a) Radial and (b) vertical position of the X point as computed in real time, (c) the distance between the X point location as computed in real time and computed off-line, (d) difference between the value of the flux at control point No. 1 as computed in real time and off-line, $\Delta\psi$, displayed as a distance computed from $\Delta\psi/(\partial\psi/\partial\ell)$, where the flux derivative is along a line between the control point and the magnetic axis, and (e) the same as (d) for control point No. 8 (the control points are labelled in Fig. 1). In (c) to (e), the solid curves show the results obtained using the best off-line reconstruction, which includes the poloidal field coil currents as fitting parameters, and the dashed curves ((d) and (e) only) use the off-line reconstruction results obtained by including the poloidal field coil currents as known values, as is the case in the real time calculation. The curves in (d) and (e) have been smoothed over 25 ms intervals so that the pairs of curves can be distinguished.

parameters. The solid curves in Figs 5(c) to (e) are examples of the difference between this calculation and the real time result. Figure 5(e) shows a change of about 4 mm that results from changing the way the poloidal field coil currents are treated, the largest change for the control points used in this single null

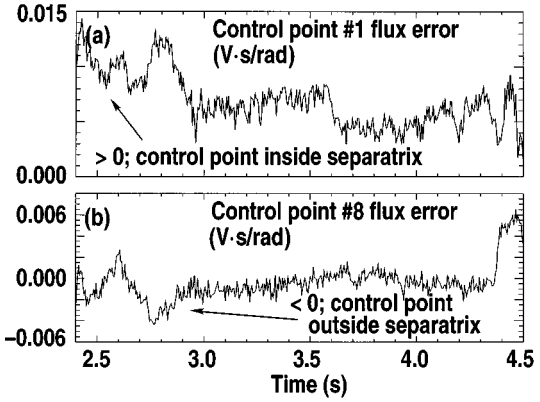

FIG. 6. Examples of the control point flux error for the discharge shown in Fig. 1. The flux errors are the difference between the flux at the control point and the flux at the reference point. Positive values indicate that the control point is inside the actual discharge boundary. (a) Control point No. 1, (b) control point No. 8.

divertor case. For the other control points, the change of the boundary location with change in treatment of the poloidal field coil currents varied between 0 and 4 mm. In this example, the X point position change was only about 1 mm. The magnitude of the effect of changing the way the coil currents are treated in the calculation will depend on the tokamak diagnostic system. In this example for the DIII-D tokamak, the effect is small because the uncertainties in the coil current measurements are relatively small.

The isoflux control algorithm is illustrated by the examples of the flux errors at two of the control points shown in Fig. 6. The flux errors, the quantities actually controlled, are the difference between the flux at the control points and the control reference flux. The flux error at control point No. 1 (Fig. 6(a)) is positive, indicating that the control point is inside the discharge boundary. This is in agreement with Fig. 1, which shows the control point locations and the boundary as computed by the off-line reconstruction. Thus, the controller will try to reduce the poloidal flux at this control point. Similarly, control point No. 8 (Fig. 6(b)) has a negative flux error at 2500 ms, the time slice in Fig. 1, so that the control point is outside the boundary. The controller will try to increase the flux there in order to correct the discharge shape. Note that the differences between the real time reconstruction and the best off-line reconstruction of the flux calculated at the control points, approximately 1×10^{-3} V · s/rad, are smaller than the flux errors shown in Fig. 6. Thus,

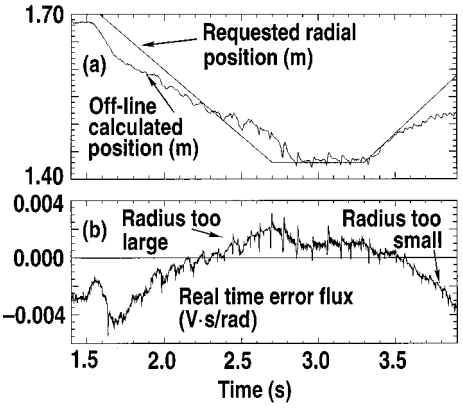

FIG. 7. Illustration of a test of strike point control: (a) requested position of the outer strike point location in a single null divertor discharge and the off-line calculation of the actual strike point location, (b) real time calculation of the difference between the flux at the requested strike point location and the flux at the X point.

the discharge shape errors in this example exist primarily because the controller has not optimized the coil currents to correct the control point flux errors.

Strike point location control, a capability essential for operation of closed divertor geometries, can be implemented relatively easily using the isoflux technique. A control point is placed at the desired strike point location. Then the strike point location is adjusted through some combination of changes in the vertical and radial position of the X point until the flux at the control point is the same as the flux at the X point. Figure 7 shows an example from a DIII-D discharge chosen to illustrate the control technique rather than accurate control. Part (a) compares the desired strike point location with the actual location obtained by the off-line reconstruction, and part (b) shows the difference between the control point flux and the flux at the X point. Within the typical 1×10^{-3} V · s/rad uncertainty in the equilibrium reconstruction, when the strike point radius is too large or too small the flux error is positive or negative, respectively, because the flux increases towards the private flux region (see Fig. 1) and decreases outside the separatrix.

6. CONCLUSION

In this article, we have described an algorithm nearly identical to a standard equilibrium reconstruction technique that is also practical to use in real time for identification of tokamak discharge parameters. It allows equilibrium parameter values for use in discharge control to be evaluated from a solution to the Grad–Shafranov tokamak equilibrium relation. Even parameters such as the safety factor profile could be available in real time. The modifications to the off-line reconstruction algorithm we have described here that make the real time execution practical affect the results, for relatively steady state conditions, on a scale of precision that is not important for practical discharge shape control. This has been demonstrated by comparing both simulations of the real time algorithm and examples of results from use of the algorithm with DIII-D tokamak discharges with reconstructions from the full off-line algorithm.

The primary limitation of the accuracy of the real time algorithm compared with the best off-line reconstruction is the characteristic time-scale for changes in the equilibrium relative to $\tau_{\mathcal{S}}$, the time required to update the starting point equilibrium for the one iteration solution. However, the discussion in Section 4 showed that the value of $\tau_{\mathcal{S}}$ affects the accuracy in locating the discharge boundary primarily during the plasma current ramps and that sufficient accuracy can be obtained by reducing $\tau_{\mathcal{S}}$. Significant boundary location errors do not appear to result from relatively rapid changes in stored energy (such as the changes in β_{p}, Fig. 3). The ability to control the boundary during large transient changes in the equilibrium on time-scales shorter than $\tau_{\mathcal{S}}$ would be limited more by the time constants of the poloidal field coil system and vacuum vessel rather than by the shape identification accuracy. In tokamaks larger than DIII-D, the characteristic times for equilibrium changes would usually be larger than that in DIII-D, so that typical values for $\tau_{\mathcal{S}}$ would not be a limitation. For smaller devices, however, values of $\tau_{\mathcal{S}}$ would probably need to be shorter than that for DIII-D. Measures such as reducing the number of diagnostic values, or using a more coarse computation grid or a faster processor, could be used to achieve this.

Advances in digital processing technology would facilitate increases in equilibrium reconstruction accuracy by reducing $\tau_{\mathcal{S}}$ and by allowing the real time algorithm to be a closer duplicate of the off-line algorithm. More than one iteration for each reconstruction solution could be executed and the poloidal field coil currents could be included as free parameters. For instance, the easiest way to implement execution of two iterations in a real time reconstruction is to first calculate $\boldsymbol{I}_{\mathrm{p}}$ and the $\mathcal{S}$ data set, completing the first iteration and providing the starting point

for both the second iteration and the first iteration of the next cycle. A complete shape control loop then implements the second iteration. The calculations for both iterations must be completed in the relatively short time period in which the poloidal field power supply commands must be updated. This two iteration calculation requires 20 to 50 times more computation than the single iteration shape control loop described in Section 4. The treatment of the poloidal field coil currents as free parameters would, for the DIII-D implementation, add approximately an additional factor of 4 in computation to the calculation of the $\mathcal{S}$ data set. Other possible improvements are increased density of the calculation grid (for instance, a 4000 element grid is typically used for routine off-line reconstruction) and implementation of a boundary tracing routine. The trade-offs between increased accuracy and increased demands on processor speed would need to be studied for the target tokamak discharges to determine which improvements to the algorithm would be the most effective.

Appendix

IMPLEMENTATION ON THE DIII-D TOKAMAK

The real time equilibrium reconstruction algorithm described in Section 4 has been successfully implemented on the DIII-D digital plasma control system (PCS) [10]. This implementation takes advantage of the feature of the algorithm that it consists primarily of a series of vector and matrix operations, the types of operation for which the processor in the PCS (an Intel i860) and other current microprocessors are optimized. Thus, the PCS processors can execute much of the algorithm at close to their theoretical maximum calculation speed (80 million floating point operations per second). Two processors are used, one dedicated to the shape control loop and one dedicated to the calculation of the $\mathcal{S}$ data set.

The time required to execute the shape control loop determines how rapidly the poloidal field coil power supply commands are updated and thus the frequency bandwidth of those commands. The required bandwidth is determined by the frequency response of the poloidal field coil power supplies and the time required for field changes to penetrate the vacuum vessel. A frequency bandwidth is required that is high enough that the feedback system can respond to rapid changes in plasma parameters, but the highest frequency necessary is determined by the filtering effect of the power supplies and the vacuum vessel. For DIII-D, the power supply frequency response is several hundred hertz and the vessel time constant is a few milliseconds.

The calculation grid and diagnostic set used for the real time implementation are approximately the same as those used in off-line calculations. A full poloidal array of 31 magnetic field probes, the full DIII-D set of 40 flux loops and a Rogowski loop are included in the diagnostic set. Provision has been made to include data from 16 channels of the MSE diagnostic in order to obtain data that will properly constrain the current profile. Thus, the total number of diagnostic measurements is typically between 70 and 88. The most coarse grid normally used for off-line calculations, 33 rows by 33 columns, is used for the real time implementation. With these parameters, typical counts of control points and one or two X points to be located, the shape control loop executes in approximately 1 to 1.5 ms, about one third of the characteristic times of the vessel and poloidal field power supplies. A typical current profile model has $n_P + n_F =$ 3–5. The calculation of $\mathcal{S}$ requires 22 to 30 ms in these cases. It is anticipated that with MSE data included, and $n_P + n_F$ increased to 7 to model the increased detail of the current profile reconstruction possible when MSE data are available, the calculation of $\mathcal{S}$ will require approximately 50 ms. These calculation times are comparable to what the example in Fig. 3 indicates would be required for DIII-D discharges.

ACKNOWLEDGEMENTS

The authors would like to thank B. Penaflor, J. Broesch, D. Baggest, T. Jensen, T. Taylor, B. Miller and the remainder of the DIII-D team for their contributions to this work. This is a report of work supported by the USDOE under Contract No. DE-AC03-89ER51114.

REFERENCES

[1] LAO, L.L., et al., Nucl. Fusion **25** (1985) 1611.
[2] HUTCHINSON, I.H., HORNE, S.F., TINIOS, G., WOLFE, S.M., GRANETZ, R.S., Fusion Technol. **30** (1996) 137.
[3] WIJNANDS, T., PARLANGE, F., COUTURIER, B., MOULIN, D., Nucl. Fusion **36** (1996) 1405.
[4] MATSUKAWA, M., HOSOGANE, N., NINOMIYA, H., Plasma Phys. Control. Fusion **34** (1992) 907.

[5] KINOSHITA, S., et al., Independent Control of Gaps in Single-Null Divertor Discharges on the DIII-D Tokamak, Rep. GA-A19584, General Atomics, San Diego, CA (1990).
[6] LISTER, J.B., SCHNURRENBERGER, H., Nucl. Fusion **31** (1991) 1291.
[7] HOFMANN, F., TONETTI, G., Nucl. Fusion **28** (1988) 519.
[8] BRAAMS, B.J., JILGE, W., LACKNER, K., Nucl. Fusion **26** (1986) 699.
[9] O'BRIEN, D.P., ELLIS, J.J., LINGERTAT, J., Nucl. Fusion **33** (1993) 467.
[10] FERRON, J.R., Rev. Sci. Instrum. **63** (1992) 5464.
[11] FERRON, J.R., et al., in Fusion Engineering (Proc. 14th Symp. San Diego, 1991), IEEE, Piscataway, NJ (1996) 761.
[12] LUXON, J.L., DAVIS, L.G., Fusion Technol. **8** (1985) 441.
[13] WROBLEWSKI, D., LAO, L.L., Rev. Sci. Instrum. **63** (1992) 5140.
[14] HOFMANN, F., JARDIN, S.C., Nucl. Fusion **30** (1990) 2013.

(Manuscript received 9 June 1997
Final manuscript accepted 17 April 1998)

E-mail address of J.R. Ferron: ferron@gav.gat.com

Subject classification: C0, Te; E0, Te